CHEMISTRY

High-performance pan-tactic polythioesters with intrinsic crystallinity and chemical recyclability

Changxia Shi[1,2], Michael L. McGraw[1], Zi-Chen Li[2], Luigi Cavallo[3], Laura Falivene[3]*, Eugene Y.-X. Chen[1]*

Three types of seemingly unyielding trade-offs have continued to challenge the rational design for circular polymers with both high chemical recyclability and high-performance properties: depolymerizability/performance, crystallinity/ductility, and stereo-disorder/crystallinity. Here, we introduce a monomer design strategy based on a bridged bicyclic thiolactone that produces stereo-disordered to perfectly stereo-ordered polythiolactones, all exhibiting high crystallinity and full chemical recyclability. These polythioesters defy aforementioned trade-offs by having an unusual set of desired properties, including intrinsic tacticity-independent crystallinity and chemical recyclability, tunable tacticities from stereo-disorder to perfect stereoregularity, as well as combined high-performance properties such as high thermal stability and crystallinity, and high mechanical strength, ductility, and toughness.

INTRODUCTION

The failure to address end-of-life issues of today's plastics has not only accelerated the depletion of finite natural resources but also caused severe worldwide plastics pollution problems and resulted in enormous energy and materials value loss in the global economy (*1*–*3*). To address this global challenge, the design of next-generation polymers must consider their afterlife issues and establish closed-loop life cycles toward a circular economy (*4*–*8*). In this context, the development of chemically recyclable polymers that can be depolymerized back to their monomer building blocks in high selectivity and purity for virgin-quality polymer reproduction offers a circular economy approach to address these dire environmental and economic issues (*9*–*16*). For example, the ring-opening polymerization (ROP) of unstrained γ-butyrolactone (GBL) leads to polyester poly(GBL) that can be completely depolymerized back to GBL in quantitative purity and yield with a low energy input (*17*, *18*). However, poly(GBL) performance properties are insufficient for common applications. To address this depolymerizability/performance trade-off, ring-fused bicyclic GBL structural derivatives were designed to enhance monomer polymerizability as well as polymer thermal stability and crystallinity without compromising the full chemical recyclability (*10*, *19*), but the resulting crystalline materials with high melting transition temperatures (T_m) are mechanically brittle, thus requiring incorporation of flexible copolymers to reach useful ductility (*20*). In addition, to afford these crystalline materials demands either stereocomplexation of the preformed enantiomeric polymers from separate pools of enantiopure monomers or the elaborate stereoselective polymerization of the racemic monomer pool. When compared to the extensively studied ROP of lactones (*21*, *22*), the ROP of thiolactones has been examined to a much lesser extent (*23*–*28*). A notable development on that front is that the ROP of chiral *N*-substituted *cis*-4-thia-L-proline thiolactones leads to polythioesters that are readily functionalizable (via the *N* site on the pyrrolidine ring) and show full chemical recyclability (*23*). However, the resulting polythioesters exhibit relatively low thermal stability with a $T_{d,5\%}$ (decomposition temperature at 5% weight loss) of ~200°C and no observable T_m, despite their chiral structure, and dilute conditions (1.0 g of polymer/100 ml of solvent) were required to achieve their full chemical recyclability. The above examples highlight the daunting challenges of designing chemically recyclable polymers that exhibit combined desirable, but often conflicting, properties into one polymer structure, as they must overcome two types of trade-offs: depolymerizability/performance and crystallinity/ductility.

For polymers containing stereogenic centers, there is also a stereo-disorder/crystallinity trade-off that must be addressed. The stereochemical order or tacticity that measures the relative stereochemical arrangement or order of neighboring stereocenters located on their main-chain backbone of polymers significantly affects their physical and mechanical properties (*29*–*31*). Although stereoregularity of polymers is neither a necessary nor a sufficient condition for their crystallinity, as a general rule for tactic polymers, tacticity determines their crystallinity; thus, high tacticity is required to pack polymer chains effectively into a (semi)crystalline domain. Therefore, higher tacticity leads to a crystalline polymer with a higher T_m, whereas stereo-disordered or atactic polymers having a random arrangement of stereocenters or even modestly tactic polymers are often amorphous. This long-standing rule highlights the importance of achieving a high degree of stereochemical control in polymer synthesis and often represents a highly demanding task for many polymerization systems, which has continuously challenged polymer chemists and captivated their attention and efforts (*32*–*36*). However, there are a few exceptions to this rule. For example, atactic poly(vinylene-*cis*-1,3-cyclopentylene) [fully hydrogenated polynorbornene (hPN)] is unexpectedly crystalline (*37*), which is attributed to the unusual ability to crystallize with good three-dimensional order (a defined unit cell) even in the presence of a high degree of local structural disorder (configurational disorder in the *cis*-cyclopentylene rings) (*38*). An obvious advantage of designing these tacticity-independent crystalline polymers is to circumvent the burden of developing

[1]Department of Chemistry, Colorado State University, Fort Collins, CO 80523-1872, USA. [2]Beijing National Laboratory for Molecular Sciences, Key Laboratory of Polymer Chemistry and Physics of Ministry of Education, Center for Soft Matter Science and Engineering, College of Chemistry and Molecular Engineering, Peking University, Beijing 100871, China. [3]King Abdullah University of Science and Technology (KAUST), Physical Sciences and Engineering Division, KAUST Catalysis Center, Thuwal 23955-6900, Saudi Arabia.
*Corresponding author. Email: eugene.chen@colostate.edu (E.Y.-X.C.); laura.falivene@gmail.com (L.F.)

exquisite stereoselective syntheses to achieve highly stereoregular, high-performance crystalline polymers.

Inspired by the above overviewed results and the presented challenges, especially the work of Yuan *et al.* (*23*) and Lee and Register (*37*), we set out to design high-performance circular polymers with both intrinsic chemical recyclability and crystallinity. Guided by the following working hypotheses, we arrived at a bridged bicyclic thiolactone monomer, 2-thiabicyclo[2.2.1]heptan-3-one ($^{[221]}$BTL), which can be prepared from a bio-based olefin carboxylic acid in 80% yield at a 50-g scale (see Materials and Methods). First, $^{[221]}$BTL should contain higher ring strain than the parent, nonpolymerizable γ-thiobutyrolactone, which should allow the ROP to proceed at room temperature (RT) with high equilibrium monomer conversions and yield high molecular weight (MW) polymers. Second, the bridged bicyclic system should provide rigidity to the polymer backbone for enhanced thermal and mechanical properties. Third, the depolymerizability and selectivity in chemical recycling of the resulting polymer poly(2-thiabicyclo[2.2.1]heptan-3-one) (PBTL) should be high since the ring closure of the five-membered thiolactone is kinetically facile and thermodynamically favored. Furthermore, the bridged bicyclic monomer exists only in the cis configuration, thus eliminating possible isomerization. Fourth, the aforementioned PBTL that also contains the cyclopentylene units, the motif leading to atactic yet crystalline hPN, could render its tacticity-independent, thus intrinsic, crystallinity, provided the unique ability to crystalize because of pseudosymmetry and long-range order present in the pantactic PBTL with all degrees of tacticity.

RESULTS

Control of tacticity, crystallinity, and topology

The results of the ROP of racemic $^{[221]}$BTL by four different catalyst/initiator systems were summarized in table S1. First, with the La-N/BnOH system, the ROP in toluene at RT with [**M**]/[La-N]/[BnOH] = 300/1/3 achieved only 57% conversion after 24 hours {La-N = La[N(SiMe$_3$)$_2$]$_3$; BnOH = benzyl alcohol, which converts in situ the La-N precatalyst to the La-OBn catalyst via facile alcoholysis (*15*); **M** = monomer}. Although the resulting PBTL has a low number-average MW (M_n) of 8.8 × 10^3 g mol^{-1} and is not stereoregular on the basis of ^{1}H and ^{13}C nuclear magnetic resonance (NMR) spectra, it unexpectedly is crystalline with a high T_m of 167°C (Fig. 1) and a heat of fusion (ΔH_f) of 25.6 J g^{-1} measured by differential scanning calorimetry (DSC) from a second heating scan at 10°C/min. Likewise, the ROP catalyzed by organic base 1,8-diazabicyclo[5.4.0]undec-7-ene (DBU) led to atactic PBTL but is semicrystalline, exhibiting a T_m of 166°C. The use of superbase 1-*tert*-butyl-4,4,4-tris(dimethylamino)-2,2-bis[tris(dimethylamino)-phosphoranylid-enamino]-2λ^5,4λ^5-catenadi (phosphazene) (^{t}Bu-P$_4$) resulted in immediate gelation with an **M** concentration of 160 mg/0.1 ml in toluene, affording also a crystalline PBTL but with a higher T_m of 176°C, while still being mostly atactic. Intriguingly, when the **M** concentration was increased to 240 mg/0.1 ml in toluene and the catalyst loading was decreased to reach a ratio of [**M**]/[^{t}Bu-P$_4$]/[BnOH] = 1000/1/1, the T_m of the resulting PBTL (M_n = 4.98 × 10^4 g mol^{-1}, $Đ$ = 1.44) increased significantly to 213°C [glass transition temperature (T_g) = 112°C], coupled with essentially perfect stereoregularity, as revealed by its

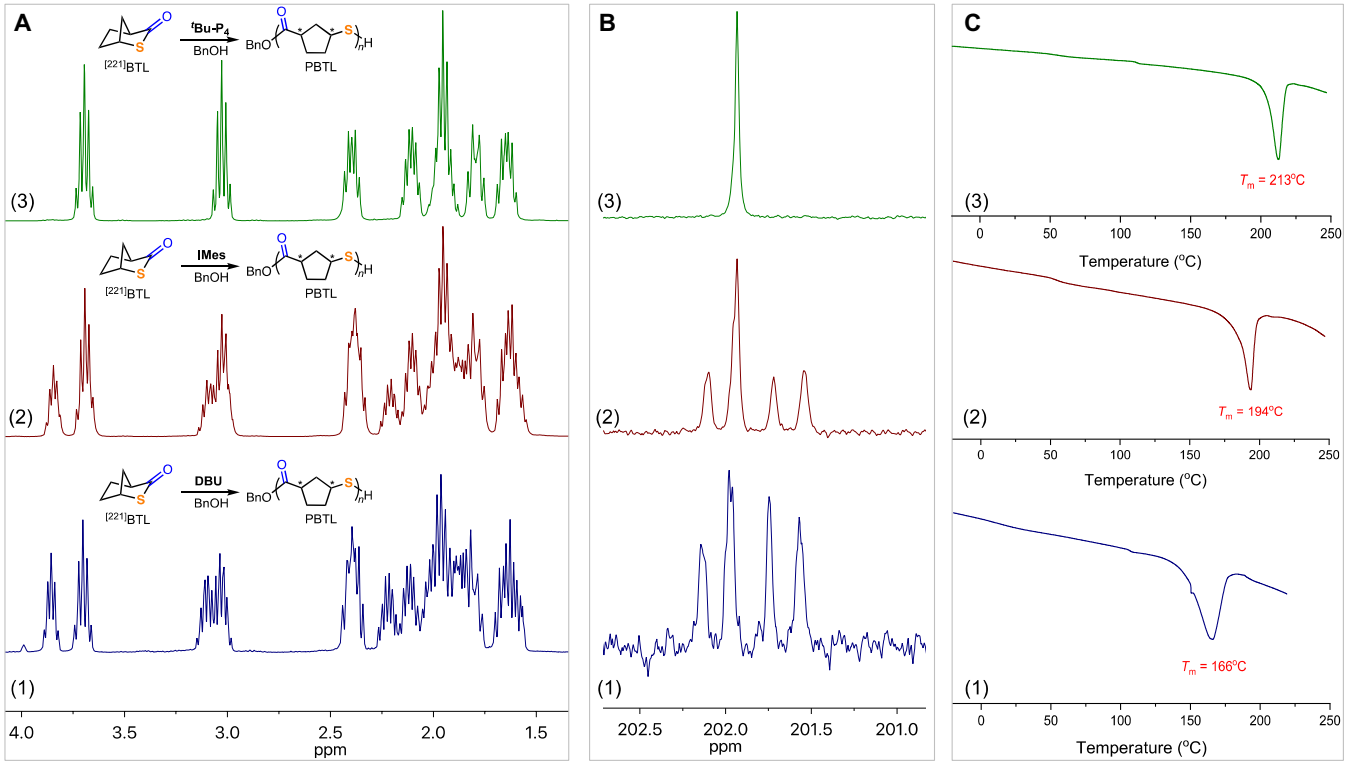

Fig. 1. NMR spectra and DSC thermograms of PBTL with varied stereoregularity. (**A**) ^{1}H NMR (25°C, $CDCl_3$) spectra. ppm, parts per million. (**B**) ^{13}C NMR (25°C, $CDCl_3$) spectra in the C═O region. (**C**) DSC curves of second heating scans at 10°C/min. PBTL samples are as follows: (1) PBTL with low (32%) tacticity by DBU; (2) PBTL with medium (45%) tacticity by IMes; and (3) PBTL with perfect (100%) tacticity by ^{t}Bu-P$_4$.

^{13}C NMR (Fig. 1B and table S1, run 4). Replacing ^{t}Bu-P$_4$ with a *N*-heterocyclic carbene (NHC), 1,3-bis(2,4,6-trimethylphenyl) imidazol-2-ylidene (IMes), the ROP with [**M**]/[IMes]/ [BnOH] = 1000/1/1 (320 mg of **M** in 0.1 ml of toluene) reached 85% in 5 min, affording a high-MW, crystalline PBTL ($M_n = 1.15 \times 10^5$ g mol^{-1}, $T_m = 194$°C; Fig. 1C). By gradually lowering the IMes catalyst loading to 0.02%, we realized essentially perfectly stereoregular PBTL with $T_m = 213$°C. The linear structure of the PBTL produced by the catalyst/BnOH systems was characterized by the end groups from their NMR spectra, which was further confirmed by matrix-assisted laser desorption/ionization–time-of-flight mass spectrometry (MALDI-TOF MS) to show the linear structure BnO—{$^{[221]}$BTL}$_n$—H (Fig. 2A).

As NHCs are well-established catalysts promoting cyclic polymer formation through zwitterionic ROP of lactones and lactides (*39*–*41*), we performed zwitterionic ROP of $^{[221]}$BTL using IMes in toluene at RT. The ROP with [**M**]/[IMes] = 100/1 (160 mg of **M** in 0.1 ml of toluene) gelled in 10 s and reached 44% conversion, with a final conversion of 72% upon quenching after 5 min. This resultant PBTL ($M_n = 6.61 \times 10^4$ g mol^{-1}, $Đ = 2.37$) is also a crystalline material, showing a T_m of 176°C (table S2, run 1). Analysis of a low-MW sample by MALDI-TOF MS (Fig. 2B) revealed no end groups, indicating that IMes mediated zwitterionic ROP to produce cyclic PBTL. To provide further experimental evidence to distinguish between the linear and cyclic PBTL topologies, gel permeation chromatography (GPC) with light scattering, refractive index, and viscosity triple detection was used to analyze and compare the PBTL materials produced by IMes with (to linear PBTL) or without (to cyclic PBTL) the BnOH initiator. A Mark-Houwink plot {i.e., double logarithmic plots of intrinsic viscosity [η] versus weight-average MW (M_w) determined by light scattering detection} of the linear PBTL produced by IMes/BnOH (table S1, run 6) and the cyclic PBTL produced by IMes alone (table S2, run 6) is depicted in Fig. 2C. As expected, cyclic PBTL exhibited a lower intrinsic viscosity than its linear analog, with a $[\eta]_{cyclic}/[\eta]_{linear}$ ratio of approximately 0.7, consistent with the theoretically predicted value for cyclic polymers (*42*).

Subsequent studies examined effects on the polymerization characteristics and cyclic PBTL properties (particularly M_n and T_m) by varying the [**M**]/[IMes] ratio (100/1 to 1000/1), **M** concentration (1.60 to 3.20 g/ml), and solvent polarity [toluene, tetrahydrofuran (THF), and dimethylformamide (DMF)]. From the results summarized in table S2, several trends can be observed. First, these polymerizations typically gel in a few seconds and are not well controlled, affording high-MW, crystalline cyclic PBTL with even a relatively low [**M**]/[IMes] ratio to 300/1: $M_n = 1.70 \times 10^5$ g mol^{-1}, $Đ = 2.78$, and $T_m = 180$°C. Second, using combined high **M** concentration (2.40 g/ml) and high [**M**]/[IMes] ratio (1000/1) conditions produced cyclic PBTL

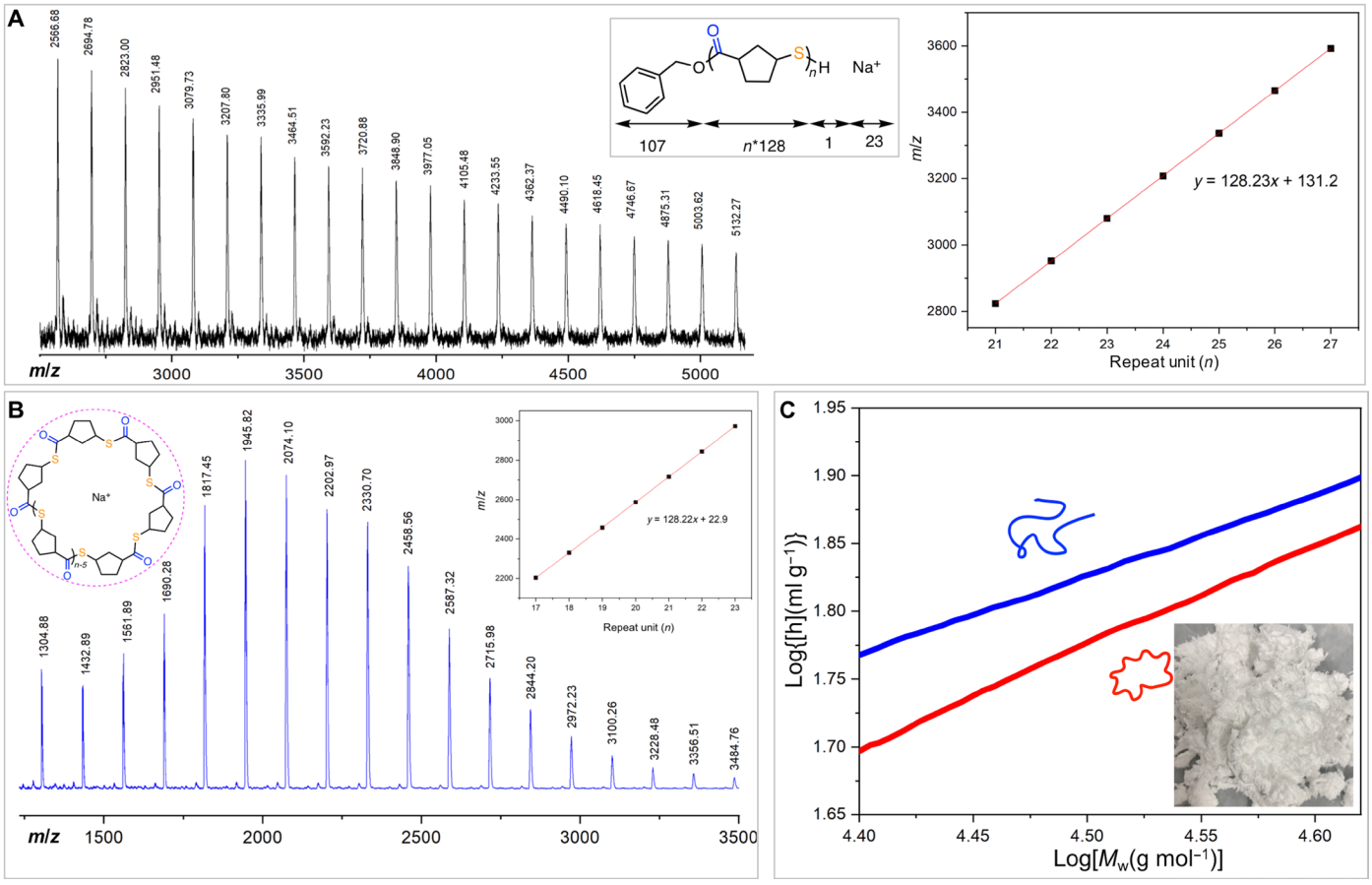

Fig. 2. Determination of topology by MALDI-TOF MS and viscosity. (**A**) MS spectrum and plot of mass/charge ratio (*m*/*z*) values versus the theoretical number of **M** repeat units for the linear PBTL produced by IMes and BnOH. (**B**) MS spectrum and plot of *m*/*z* values versus the theoretical number of **M** repeat units for the cyclic PBTL produced by IMes alone. (**C**) Double logarithm (Mark-Houwink) plots of intrinsic viscosity [η] versus M_w of the linear (blue line) and cyclic (red line) PBTL samples produced by IMes with BnOH and without BnOH. Inset: a photograph of isolated cyclic PBTL.

with essentially perfect tacticity, as characterized by the highest T_m of 213°C and ^{13}C NMR spectra. Third, changing the solvent from toluene to THF, while using high **M** concentration and [**M**]/[IMes] ratio conditions, can also lead to perfectly tactic cyclic PBTL, but the ROP in the most polar solvent of this series (DMF) led to erosion of tacticity to only 30% (vide infra).

Stereomicrostructures and stereocontrol mechanism

One critical observation and clue to the origin of stereoselectivity is the appearance of four ^{13}C peaks in the carbonyl region of lower T_m (less stereoregular) PBTL materials (Fig. 3). Considering that only one of the four peaks [at 202.0 parts per million (ppm)] appears in the highest tacticity (100%) and T_m (213°C) sample, we attribute the other three peaks (202.2, 201.8, and 201.6 ppm) to stereoerrors. Next, to formulate any reasonable explanation for the observation of only four peaks, we make a critical assumption that these carbonyl ^{13}C signals must be diads, not triads. For diads, there should be 16 possible stereochemical outcomes (2^4) or 8 pairs of observable enantiomers with distinct chemical shifts. Therefore, there must be a chemical explanation for the exclusion of four other pairs of enantiomers. All eight possible diastereomers (their enantiomers not shown) at the diad level are shown in Fig. 3A, which are broken into two sets (**I** and **II**) of four. Diastereomers **1** and **5** represent the two possible parent enantiomers that arise from inherent chain-end stereoselectivity inherited from the unracemized enantiomeric cis monomer. It makes sense to split them up into these two scenarios if, and only if, the chiral center adjacent to the sulfur does not racemize (note that in each set, the stereocenters adjacent to the sulfur atom do not change). Regardless of what the parent chirality is, *cis*/*cis* threodisyndiotactic **1** [(*R*,*S*)(*S*,*R*)] or *cis*/*cis* threodiisotactic **5** [(*R*,*S*)(*R*,*S*)], we can still infer that racemization between any of the diastereomers in scenarios **I** to **II** requires a flip in chirality at one of the stereocenters adjacent to a sulfur. Therefore, under the above assumption, we can consider the two scenarios as mutually exclusive and thus provide a well-reasoned chemical explanation for the exclusion of the four statistically possible but missing peaks. To understand which scenario can be ruled out, we performed density functional theory (DFT) calculations and reported relative energies of the eight diads in Fig. 3A. From a thermodynamic perspective, group **I** diastereomers are calculated to be more stable than the ones in group **II**. Specifically, threodisyndiotactic **1**, representing the tacticity formed by the stereoselective chain growth, is about 2 kcal/mol more stable than threodiisotactic **5** and, among the racemized chains, *trans*/*trans* **4** is the favored one. The kinetic results that emerged from the DFT analysis of mechanistic pathways discussed below show that the selective formation of **1** is also kinetically favored.

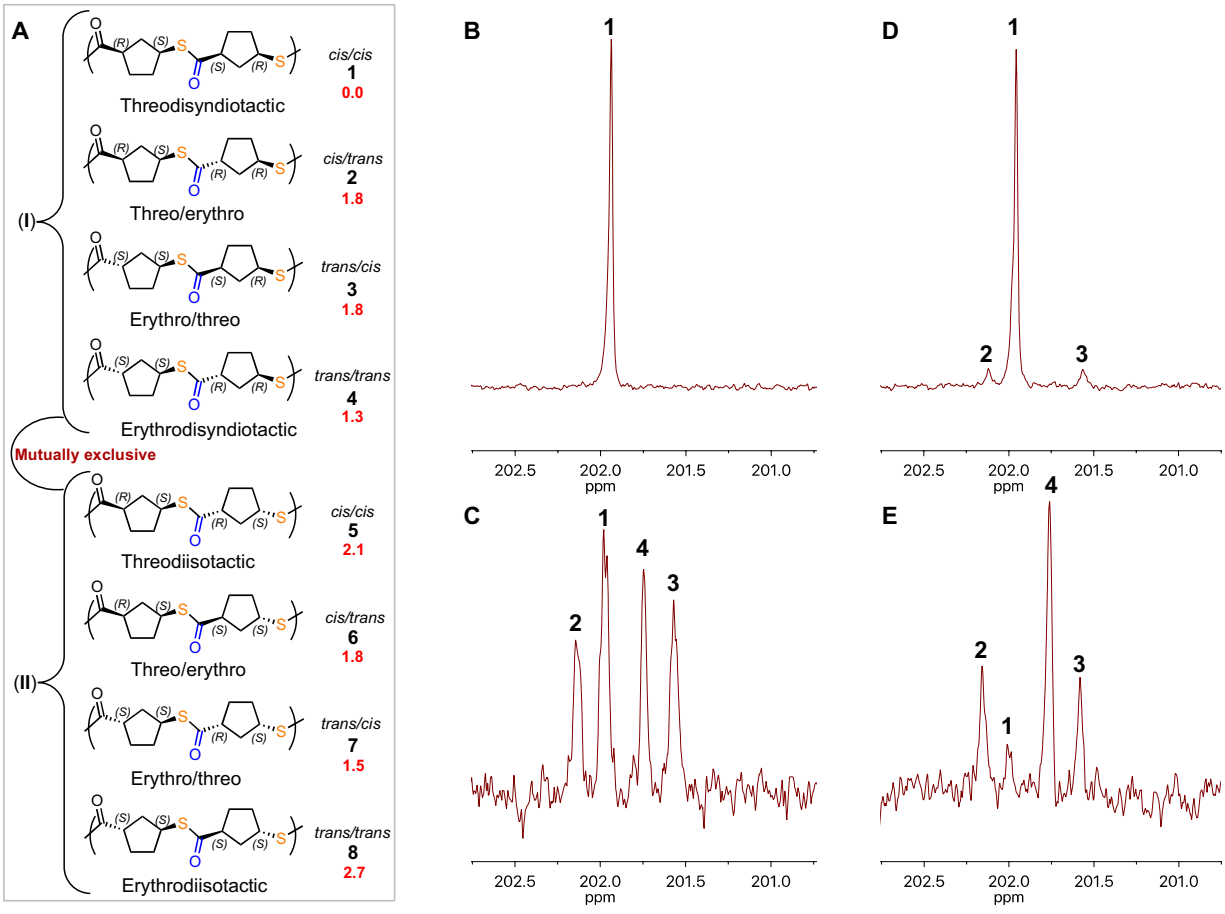

Fig. 3. Tentative assignments of stereomicrostructures of PBTL and ^{13}C NMR spectra. (**A**) Structures of all possible stereo-arrangements (tacticities) in diads (enantiomers not shown) and DFT calculated relative energies (numbers in red; kcal/mol). (**B**) PBTL produced by IMes (table S2, run 8). (**C**) PBTL produced by DBU (table S1, run 2). (**D**) PBTL produced by IMes (table S1, run 8). (**E**) PBTL produced by ^{t}Bu-P$_4$, [**M**]/[^{t}Bu-P$_4$]/[BnOH] = 100/1/1, 0.80 g/ml.

The above rationalization can also explain the two outside peaks (202.2 and 201.6 ppm), which are stereoerrors, that apparently always have similar integration (Fig. 3, C to E). There are two cis/trans diastereomers, **2** and **3**. Since each ^{13}C peak is representing one specific carbonyl carbon that can either be on the cis ring or the trans ring within the cis/trans diad and since these are two chemically different carbons, they would logically be similar in abundance and therefore have similar integration in every case. Last, the inside/right peak (**4**) represents the trans/trans diastereomer. This assignment is consistent with Fig. 3E for the PBTL produced by ^{t}Bu-P$_4$ under more dilute conditions, where the trans/trans peak is highest in intensity because of facile racemization under these conditions.

We propose a stereospecific chain-end control mechanism on the basis of inherent steric differences in the pro-(*S*) and pro-(*R*) faces of any incoming $^{[221]}$BTL molecule, coupled with the chirality of any propagating PBTL anionic chain end. Stereomistakes are caused by racemization of the stereocenter α- to a PBTL carbonyl by an equivalent of free base. In addition, while one might expect stronger bases to produce more stereoerrors, the results from table S1 indicated that stronger bases are actually the most stereoselective. This counterintuitive observation can be explained by the absolute concentration of the free base being lower in the case of a stronger base such as ^{t}Bu-P$_4$ in comparison to a weaker base such as DBU. This hypothesis is also supported by the higher T_m's observed at higher [**M**]/[B:] ratios, where the absolute concentration of the free base must be lower. However, current evidence could not allow us to conclusively rule out an alternative hypothesis that the higher stereoselectivity achieved by the stronger base ^{t}Bu-P$_4$ is due, at least partially, to its much greater steric hindrance (thus, bulkier resulting conjugate-acid anion). Deconvolution of the steric bulk from the basicity of bases requires further structure/reactivity studies. Overall, the experimental observations and analyses led to three critical conclusions: (i) The thiolate anion is not a strong enough base to racemize the α-carbonyl carbon; (ii) the proton adjacent to the sulfur is not acidic enough to racemize; and (iii) stronger bases are less prone to racemize the polymer chain because they are more likely to exist in the innocuous protonated form.

To address the above mechanistic hypotheses, DFT calculations were carried out for the ROP of racemic $^{[221]}$BTL with ^{t}Bu-P$_4$. Starting from the anionic thiolate propagating chain **A** stabilized by electrostatic interaction with the protonated base [BH]$^+$ (Fig. 4A), the next monomer addition occurs through a nucleophilic attack by the thiolate on the carbonyl of the monomer with concomitant ring opening and reformation of a longer thiolate chain. The reaction of the pro-(*S*) face of $^{[221]}$BTL requires a barrier of only 8.5 kcal/mol, 4.6 kcal/mol lower than that for the pro-(*R*) face, confirming a completely stereospecific chain-end control. Moreover, this kinetic barrier difference shows that the selective formation of diad **1** [(*R*,*S*)(*S*,*R*)] over **5** [(*R*,*S*)(*R*,*S*)] is both kinetically and thermodynamically favored.

Next, we investigated the possible pathways leading to stereoerrors. The proton exchange between the thiolate anion at the chain end and the base creates an equilibrium between ion pair **A** and neutral thiol and base pair **B** (Fig. 4A). As expected, the formation of **B** is disfavored, but, when formed, **B** can facilitate racemization at the α-carbonyl carbon through abstraction of the proton by the released base, which has a barrier of 13 kcal/mol leading to **C** (only 3.6 kcal/mol higher in energy than **B**). On the other hand, analogous product **D**, generated by racemization at the stereocenter adjacent to sulfur, is very high in energy (41.4 kcal/mol higher than **A** or 28.4 kcal/mol higher than **B**); thus, its formation can be ruled out. Further, chain growth from **C** occurs more rapidly for the newly formed trans chain end that propagates with a barrier lower by almost 2 kcal/mol with respect to the regular chain end. These results support the formation of a predominantly trans/trans structure (**4** in Fig. 3A) and its existence as a kinetic product when the reaction conditions were used such that extensive racemization can occur (Fig. 3E).

Furthermore, we examined both initiation and propagation pathways for the IMes-catalyzed cyclic PBTL formation in toluene (Fig. 4B). The initiating nucleophilic attack of IMes to the carbonyl carbon of $^{[221]}$BTL requires a barrier of 12.6 kcal/mol, leading to ring-opened zwitterionic adduct **E** that is 6.6 kcal/mol higher in energy than the reactants. The following monomer addition is also stereoselective

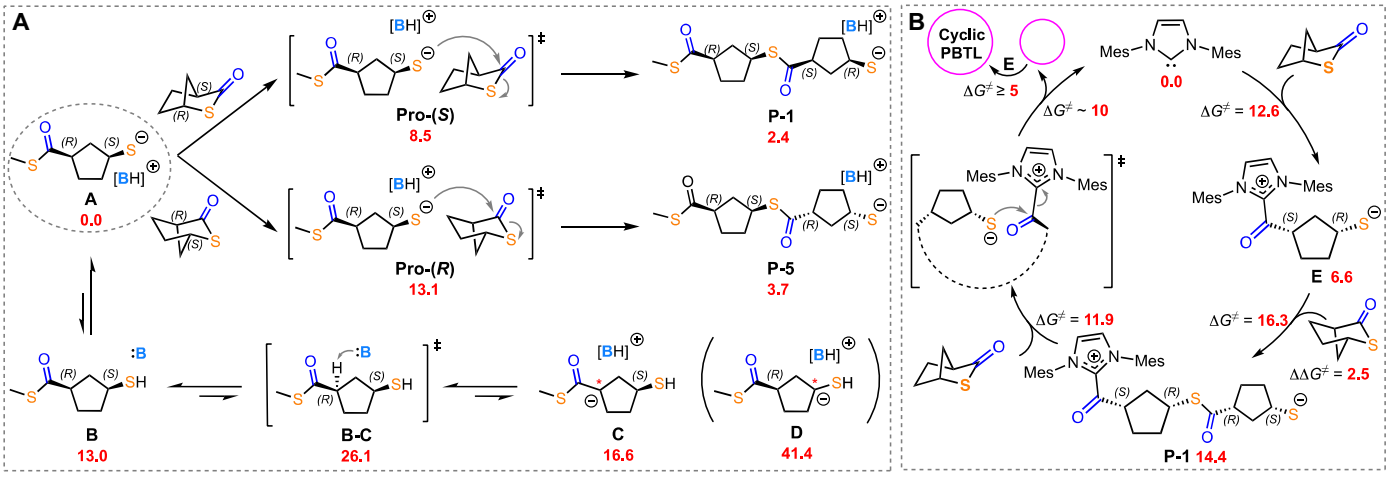

Fig. 4. Proposed stereospecific ROP mechanism. (**A**) Stereospecific ROP of $^{[221]}$BTL into perfectly stereoregular linear PBTL (**P-1**) with threo-disyndiotacticity by chain-end control (top) and stereoerror formation via racemization at the stereocenter adjacent to the carbonyl by free base present in the system (bottom). (**B**) Zwitterionic initiation, propagation, chain extension, and cyclization fundamental steps for cyclic PBTL formation by IMes. DFT calculated relative free energies in toluene (kcal/mol) reported by numbers in red, and $\Delta G^{\neq}$ calculated as the free energy difference between each transition state and its preceding minima.

($\Delta\Delta G^{\neq}$ of 2.5 kcal/mol between the transition states for the two faces of the monomer) with a relative energy barrier of 16.3 kcal/mol for the favored enantiomer, which also leads to the thermodynamically favored diad (threodisyndiotactic **P-1**). The propagation step for the favored stereoselective pathway requires a relative energy barrier of 11.9 kcal/mol for the addition of the third monomer (Fig. 5A). The lower energy required in this step with respect to the previous one correlates well with the strength of the ion pair formed by the growing chain. In the initial adduct **E**, the end-to-end distance is very short, i.e., 2.10 Å, indicating a very tight ion pair, but after at least two monomer units have been inserted into the chain, the ion pair is much weaker with an end-to-end distance of 2.88 Å. A complete chain propagation scenario contemplates also possible intermolecular chain transfer by coupling of two growing chains and regeneration of the catalyst with an energy barrier of only 9.9 kcal/mol (Fig. 5B). The "truncated" model used, which is based on a hypothesis that there is no ring strain for big rings, allows one to ignore the repeat units and compute only the reaction between the two chain ends to avoid the conformational issues caused from the modeling of long chains. This chain transfer step competes with the analog intramolecular cyclization step that is approximated to have a similarly low energy barrier since the same truncated model can be used to model the chemistry of both the chain transfer reactions. Last, we considered the possible reactivation of small rings by active propagating species **E** or its homologs to test the possibility for cyclized chains to reenter the propagation cycle and lead to a further increase of MW (Fig. 5C). Considering a ring formed by two monomer units, the energy barrier required for the propagating chain to reopen the ring by **E** amounts to only 5 kcal/mol (which will increase as the ring size increases), supporting the facile formation of high MW chains even when there are small rings formed during the initial stage of polymerization. Thus, the lack of control and high MW/Đ can be understood as a broad probability distribution encompassing inter/intramolecular chain transfer and macrocyclic ring opening/ring closing.

Last, we also compared the computed $\Delta\Delta G^{\neq}$ values in toluene and DMF for the monomer addition step (**E** to **P-1**; Fig. 4B). The calculated $\Delta\Delta G^{\neq}$ value between the two competing transition states was reduced from 2.5 kcal/mol in toluene to only 1.2 kcal/mol in DMF, in agreement with the low stereoselectivity observed in DMF experimentally. We noticed that the stereoselection is inverted with the chain preferring to select the monomer of the opposite chirality in DMF than in toluene. Looking closely to the geometries of the two transition states, it emerges that the structure having the shorter distance between the positively and the negatively charged chain ends (i.e., the tighter ion pair) is strongly favored in an apolar solvent such as toluene, but this tight ion pairing becomes disfavored in a polar solvent such as DMF where the solvent–chain end interactions are stronger and compete with the in-chain interactions.

Materials properties of PBTL of varying topology and tacticity

The thermal stability of linear and cyclic PBTL materials were examined by thermogravimetric analysis (TGA) for their $T_{d,5\%}$ and T_{max} (a maximum rate decomposition temperature) values. Both linear and cyclic PBTL materials exhibit high thermal stability, with $T_{d,5\%} > 320$°C and with cyclic PBTL (absent of chain ends) showing somewhat higher $T_{d,5\%}$ than the linear PBTL. For example, cyclic PBTL produced by IMes alone was analyzed to have $T_{d,5\%} = 328$°C (Fig. 6A), which is 7°C higher than the linear PBTL obtained with [^{t}Bu-P$_4$ + BnOH] (fig. S67A).

Mechanical properties of crystalline cyclic PBTL materials with two different T_m values (different tacticities) prepared from the ROP of racemic $^{[221]}$BTL by IMes at a multigram scale were examined by tensile testing. Dog bone–shaped specimens of PBTL$_{178}$ (subscripted 178 denotes its T_m value of 178°C; $M_n = 9.87 \times 10^4$ g mol^{-1}) and PBTL$_{189}$ ($M_n = 2.28 \times 10^5$ g mol^{-1}) were prepared by solvent casting, followed by extensive drying in open air and a heated vacuum oven at 100°C. Despite being highly crystalline with high T_m values, both polythioesters are ductile, with elongation at break reaching greater than 200%: 222 ± 5% for PBTL$_{178}$ and 233 ± 22% for PBTL$_{189}$ (Fig. 6B). They are also hard and strong materials, with high Young's modulus and ultimate tensile strength of $E = 2.00 \pm 0.18$ GPa and $\sigma_B = 41.4 \pm 3.0$ MPa for PBTL$_{189}$ and $E = 1.38 \pm 0.17$ GPa and $\sigma_B = 36.3 \pm 3.5$ MPa for PBTL$_{178}$. Overall, they can be characterized as hard, strong, ductile, and tough plastics, with PBTL of the higher MW and T_m outperforming the one with lower values. Applying different annealing temperatures provides another strategy to modulate the properties of PBTL to meet different application demands. For example, annealing the above specimens at 140°C, which is higher than their crystallization temperatures (~130°C), yielded different mechanical properties. Specifically, PBTL$_{189}$, when annealed at 140°C, resulted in a material with ~40% higher Young's modulus ($E = 2.79 \pm 0.16$ GPa) and ~19% higher tensile strength ($\sigma_B = 49.1 \pm 3.0$ MPa) compared to the material annealed at 100°C (fig. S68). DSC measurements of the PBTL sample before and after the annealing showed that, after the annealing, the heat fusion from the first heating scans was enhanced by 8.4 J/g and the transition for T_g also became obscure, both observations of which point to an increase in crystallinity after annealing.

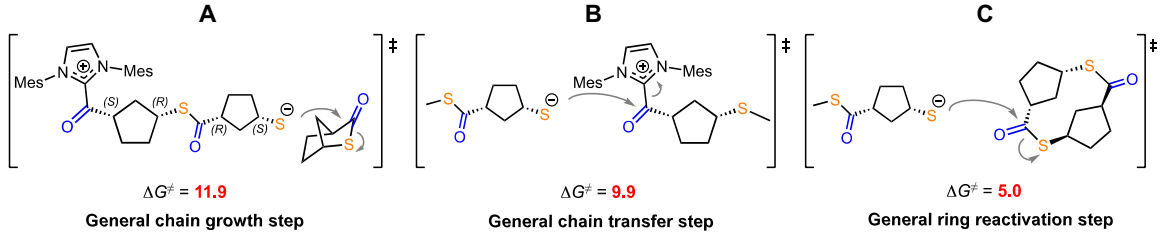

Fig. 5. Proposed chain growth, transfer, and reactivation mechanisms in the ROP of $^{[221]}$BTL by IMes. (**A**) General chain growth step following the initiation step. (**B**) Intermolecular chain transfer by coupling of two growing chains and regeneration of the IMes catalyst. (**C**) Reactivation of small rings (represented by the smallest possible ring) by active propagating species for cyclized chains to reenter the propagation cycle and lead to a further increase of the MW. DFT calculated energy barriers ($\Delta G^{\neq}$) in toluene (kcal/mol), reported as the free energy difference between each transition state and its preceding minima.

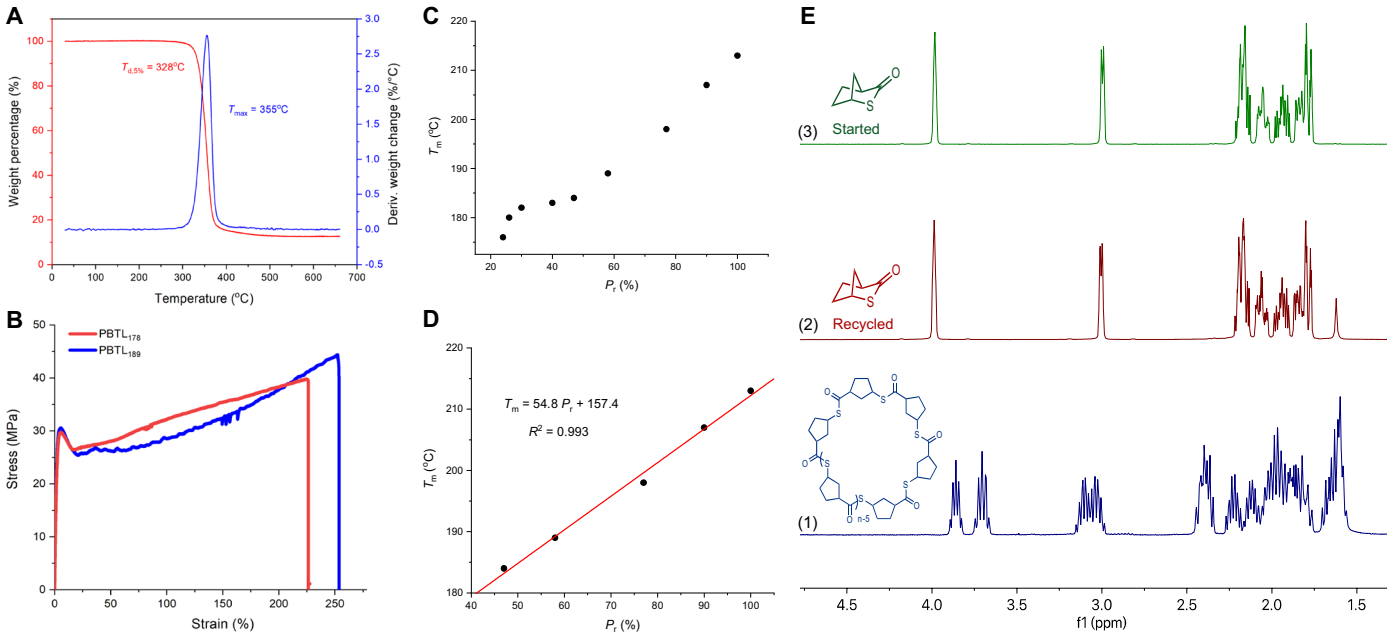

Fig. 6. Thermal and mechanical properties as well as intrinsic crystallinity and recyclability. (**A**) TGA curves of cyclic PBTL. (**B**) Stress-strain curves for $PBTL_{178}$ (T_m = 178°C and $M_n = 9.87 \times 10^4$ g mol^{-1}) and $PBTL_{189}$ (T_m = 189°C and $M_n = 2.28 \times 10^5$ g mol^{-1}). (**C**) T_m values as a function of tacticity for the cyclic PBTL materials produced by IMes. (**D**) Correlation between T_m and tacticity values for the cyclic PBTL materials produced by IMes in the linear region. (**E**) Overlays of ^{1}H NMR spectra (25°C; $CDCl_3$; residual solvent peaks at 7.26 and 1.56 ppm for $CHCl_3$ and H_2O, respectively): (1) cyclic PBTL before depolymerization; (2) the colorless solid product recovered after depolymerization (sublimation setup with La-N catalyst at 100°C for 24 hours); and (3) pure starting $^{[221]}$BTL for comparison.

Thermomechanical properties of two PBTL samples with T_m = 178°C ($M_n = 9.87 \times 10^4$ g mol^{-1}) and T_m = 213°C ($M_n = 3.33 \times 10^4$ g mol^{-1}) were examined by dynamic mechanical analysis (DMA) in a tension film mode. The thermomechanical spectra of $PBTL_{178}$ (fig. S67B) and $PBTL_{213}$ show that both samples exhibited a high storage modulus (E') at RT, although E' (1.08 ± 0.14 GPa) of $PBTL_{213}$ is somewhat higher than that (0.93 ± 0.06 GPa) of $PBTL_{178}$. On the other hand, E' of both materials only decreased by about one order of magnitude after T_g, and the materials still maintained a high E' in the rubbery plateau until reaching a flow temperature of above their T_m values, characteristic of a semicrystalline material. The α-transition temperature, given by the maximum value of tan δ [the loss modulus/storage modulus ratio (E''/E')] measured by DMA was 68°C for $PBTL_{178}$ and 98°C for $PBTL_{213}$, which is lower than the T_g (112°C for $PBTL_{213}$) measured by DSC.

Powder x-ray diffraction profiles of the cyclic PBTL with varying tacticities, as reflected by different T_m values, were also obtained. The main diffraction peak of each PBTL sample was similar, appearing at 2θ of 19.1°, corresponding to a d spacing of 4.6 nm. With increasing the tacticity from $PBTL_{183}$ to $PBTL_{207}$ to $PBTL_{213}$ with perfect tacticity, the minor diffraction peak at 11.7° grows gradually (fig. S67C), and both peaks become somewhat sharper, consistent with increasing the crystallinity and T_m values. Overlays of Fourier transform infrared (FTIR) spectra in the carbonyl stretching region of these three PBTL samples (fig. S67D) revealed a red shift of the C=O stretching frequency ($\nu_{C=O}$) for the perfectly tactic $PBTL_{213}$ to a wave number 3 cm^{-1} lower than that for the lower tactic PBTL samples.

Intrinsic crystallinity and chemical recyclability

A remarkable feature of the PBTL material is its intrinsic crystallinity, exhibiting a high T_m ranging from the lowest 166°C to the highest 213°C, regardless of topology (linear or cyclic) or tacticity (from low 20% to perfect 100%). It is worth noting here that the tacticity further modulates the crystallinity, as shown by the dependence of T_m values on tacticity. Taking the cyclic PBTL material as an example, a plot of T_m versus tacticity displays an overall upward trend (Fig. 6C), and there shows an apparent linear correlation after the tacticity reaches about 50% (Fig. 6D), with T_m (°C) = 54.8 P_r + 157.4 (R^2 = 0.993) and a calculated maximum T_m of 212.2°C at 100% P_r. If all data points (including those with tacticity lower than 50%) are plotted, then the relationship becomes: T_m (°C) = 44.6 P_r + 165.8 (R^2 = 0.984), giving a calculated minimum T_m of 165.8°C, which can be ascribed to the PBTL's intrinsic crystallinity. Experimentally, considering more than 100 PBTL samples varying in tacticity and T_m values that we have generated throughout this study, the highest and lowest T_m ever observed was consistently 213° and 166°C, respectively. These results show that this class of PBTL polymers exhibits the unusual ability to crystallize, even with a high degree of stereochemical disorder.

Another desired property of PBTL materials is their intrinsic chemical recyclability for a closed-loop life cycle. To quantify the polymerizability of $^{[221]}$BTL and also guide the PBTL depolymerization conditions, thermodynamics of the $^{[221]}$BTL polymerization were probed using the polymerization with [**M**]/[IMes] = 100/1 and $[\mathbf{M}]_0$ = 3.0 M in toluene-d_8 via variable temperature NMR. The equilibrium monomer concentration, $[\mathbf{M}]_{eq}$, obtained by plotting $[\mathbf{M}]_t$ as a function of time until [**M**] became constant, was measured to be 2.55, 2.07, 1.65, 1.32, and 1.05 M for 20°, 10°, 0°, −10°, and −20°C, respectively. The van't Hoff plot of $\ln[\mathbf{M}]_{eq}$ versus $1/T$ gave a straight line with a slope of −1.69 and an intercept of 6.70 (fig. S73), from which thermodynamic parameters were calculated to be $\Delta H°_p$ = −14.1 kJ mol^{-1} and $\Delta S°_p$ = −55.7 J mol^{-1} K^{-1}. The ceiling temperature (T_c) was calculated to be 253 K (−20°C) at $[\mathbf{M}]_0$ = 1.0 M or 385 K (112°C) at $[\mathbf{M}]_0$ = 10.0 M.

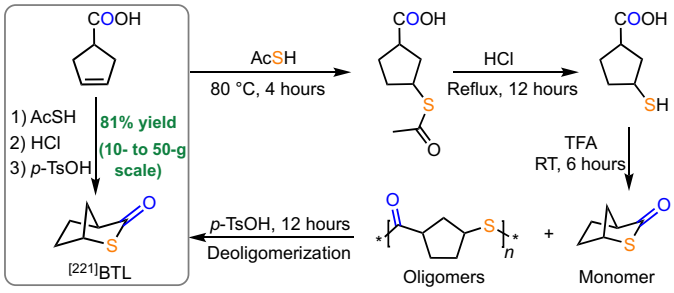

Fig. 7. Outlined one-pot synthesis of monomer [221]BTL.

The chemical recyclability of PBTL was examined by both bulk and solution depolymerization methods. First, we used bulk depolymerization at 100°C in the presence of a catalytic amount of La-N via a sublimation setup. PBTL depolymerized cleanly into pure monomer [221]BTL with >90% isolated yield after in 24 hours (Fig. 6E). Next, according to the above-obtained thermodynamic parameters, T_c = 303 K (30°C) at $[\mathbf{M}]_0$ = 3.0 M and T_c = 282 K (9°C) at $[\mathbf{M}]_0$ = 2.0 M, we investigated solution depolymerization at RT with a catalyst. When PBTL was mixed with IMes [2.3 weight % (wt %)] in toluene (2.0 M) at RT, after 10 min, PBTL depolymerized quantitatively into pure monomer [221]BTL based on ^{1}H NMR in toluene-d_8 (fig. S75). The depolymerization at a gram scale was also successfully carried out. Since [221]BTL exists only in the cis configuration, it is free of contamination because of absence of possible isomerization. The recycled pure [221]BTL can then be directly repolymerized into PBTL (table S1, run 5), thereby demonstrating a closed-loop life cycle of the PBTL materials.

DISCUSSION

In summary, we report a unique class of polythioester materials derived from the bridged bicyclic [221]BTL, which have both intrinsic chemical recyclability and crystallinity as well as an unusual set of combined high-performance properties such as high thermal stability, crystallinity, strength, ductility, and toughness. This discovery is notable because accessing such a set of desired properties typically requires composites of materials due to structure/property trade-offs. Several notable characteristics of the current designer monomer are responsible for its unique polymerization characteristics and performances of its resulting polythioesters: (i) The bridged bicyclic monomer framework increases not only the polymerizability and stereoselectivity but also the chemical recyclability and selectivity due to its enhanced ring strain and the presence of the five-member lactone ring restricted to the cis configuration; (ii) the bridged bicyclic system provides the rigidity in the polymer backbone for enhanced thermal and mechanical properties; and (iii) the cyclopentylene rings and sulfur in the polymer render tacticity-independent intrinsic crystallinity.

MATERIALS AND METHODS

Materials

High-performance liquid chromatography (HPLC)–grade organic solvents were first sparged extensively with nitrogen during filling 20 liters of solvent reservoirs and then dried by passage through activated alumina (for THF and dichloromethane) followed by passage through Q-5–supported copper catalyst (for toluene and hexanes) stainless steel columns. HPLC-grade *N,N*-DMF was degassed and dried over CaH_2 overnight, followed by vacuum distillation (CaH_2 was removed before distillation). Toluene-d_8 was dried over sodium/potassium alloy and vacuum-distilled or filtered, whereas CD_2Cl_2 and $CDCl_3$ were dried over activated Davison 4-Å molecular sieves.

Organic bases ^{t}BU-P$_4$ (~0.8 M in hexane) and IMes were purchased from Aldrich Chemical Co. and TCI, respectively, and used as received. La-N was purchased from Aldrich Chemical Co. and used as received. BnOH and DBU were purchased from ThermoFisher Scientific and Aldrich Chemical Co., respectively, which were purified by distillation over CaH_2 and stored over activated Davison 4-Å molecular sieves. 3-Cyclopentene-1-carboxylic acid was purchased from Accela ChemBio Inc. and used as received, while thioacetic acid, bromotrimethylsilane, and tris(trimethylsilyl)silane were purchased from Acros Organics and used as received. The monomer was purified and dried by recrystallization in hexanes and sublimation twice before polymerization runs and stored in the glovebox for further use.

Synthesis of monomer [221]BTL

The fundamental steps involved in the synthesis of monomer [221]BTL are depicted in Fig. 7. Thioacetic acid (11.9 ml, 170 mmol) was added to 3-cyclopentene-1-carboxylic acid (12.7 g, 113 mmol) at RT. The reaction mixture was heated at 80°C for 4 hours. After cooling to RT, 6.0 M HCl(aq) (100 ml) was added to the reaction mixture and heated at reflux for 12 hours. After drying under vacuum, acetic anhydride (20 ml) and trifluoroacetic anhydride (TFA) (2.0 ml) were added to the reaction mixture, and the mixture was stirred at RT for 6 hours. After the reaction mixture was concentrated under reduced pressure, 200 ml of toluene and *para*-toluenesulfonic acid (2.1 g, 10%) was added. The reaction mixture was heated to reflux with azeotropic removal of water, using a Dean-Stark trap. After 12 hours, the reaction mixture was cooled to RT, and the crude product was purified by silica gel column chromatography (1:20 EtOAc/hexanes) to afford pure [221]BTL (11.7 g, 81%), as a white solid (T_m = 104°C). The synthesis carried out on a 50-g scale afforded a similar yield. ^{1}H NMR (400 MHz, $CDCl_3$), fig. S1: δ 3.98 (t, J = 3.3 Hz, 1H), 3.00 (dt, J = 5.3, 1.6 Hz, 1H), 2.27 to 2.11 (m, 2H), 2.05 (dddd, J = 12.8, 8.9, 4.1, 2.3 Hz, 1H), 2.00 to 1.88 (m, 1H), and 1.87 to 1.73 (m, 2H). ^{13}C NMR (101 MHz, $CDCl_3$), fig. S2: δ 208.60, 51.39, 50.14, 43.48, 31.37, and 24.04.

General polymerization procedures

Polymerizations were performed in 5 ml of dried glass reactors inside an inert gas (Ar or N_2)–filled glovebox at ambient temperature (~25°C) runs. In a typical polymerization reaction, the catalyst or initiator was added to the vigorously stirred monomer; when BnOH was used as the initiator, it was premixed with the catalyst before adding to monomer. After a desired period of time indicated in the polymerization tables (tables S1 and S2), the polymerization was quenched by addition of $CHCl_3$ acidified with benzoic acid (10 mg/ml). The quenched mixture was precipitated into methanol, filtered, and washed with methanol; this procedure was repeated three times to ensure any catalyst residue or unreacted monomer was removed. The polymer was dried in a vacuum oven at 80°C for 3 days to a constant weight.

Absolute MW measurements

Measurements of polymer absolute weight-average molecular weight (M_w), number-average molecular weight (M_n), and MW distributions

or dispersity indices (Đ = M_w/M_n) were performed via GPC. The GPC instrument consisted of an Agilent HPLC system equipped with one guard column and two PLgel 5-μm mixed-C gel permeation columns and coupled with a Wyatt DAWN HELEOS II multi (18)–angle light scattering detector and a Wyatt Optilab T-rEX dRI detector; the analysis was performed at 40°C using chloroform as the eluent at a flow rate of 1.0 ml/min, using Wyatt ASTRA 7.1.2 MW characterization software. The refractive index increments (d*n*/d*c*) of the linear and cyclic PBTL were determined to be 0.1638 ± 0.0097 ml/g and 0.1516 ± 0.0061 ml/g, respectively, obtained by batch experiments using the Wyatt Optilab T-rEX dRI detector and calculated using the ASTRA software. Polymer solutions were prepared in chloroform and injected into the dRI detector by Harvard Apparatus pump 11 at a flow rate of 0.1 ml/min. A series of known concentrations were injected, and the change in refractive index was measured to obtain a plot of change in refractive index versus change in concentration ranging from 0.5 to 5.0 mg/ml. The slope from a linear fitting of the data was the d*n*/d*c* of the polymer.

Spectroscopic characterizations

The isolated low MW samples were analyzed by MALDI-TOF MS; the experiment was performed on an Ultraflex MALDI-TOF mass spectrometer (Bruker Daltonics) operated in a positive-ion, reflector mode using a neodymium-doped yttrium aluminum garnet laser at 355 nm and 25 kV of accelerating voltage. A thin layer of a 1% NaI solution was first deposited on the target plate, followed by 0.6 μl of both sample and matrix (dithranol, 10 mg/ml in 50% acetonitrile, 0.1% trifluoroacetic acid). External calibration was done using a peptide calibration mixture (four to six peptides) on a spot adjacent to the sample. The raw data were processed in the FlexAnalysis software (version 2.4, Bruker Daltonics).

X-ray powder patterns of the polymers were obtained with a Thermo Scintag X-2 powder x-ray diffractometer with Cu radiation. Before analysis, specimens were cooled by liquid N_2 and grinded until a fine white powder was obtained. FTIR spectroscopy was performed on a Thermo Scientific (Nicolet iS50) FTIR spectrometer equipped with a diamond attenuated total reflectance at RT in the range of 550 to 4000 cm^{-1}.

NMR spectra were recorded on a Varian Inova 400-MHz (FT 400 MHz, ^1H; 100 MHz, ^{13}C) or a 500-MHz spectrometer. Chemical shifts for all spectra were referenced to internal solvent resonances and were reported as parts per million relative to $SiMe_4$.

Measurements of thermodynamic parameters

In a glovebox under an argon atmosphere, an NMR tube was charged with IMes (4.56 mg, 0.015 mmol) and 0.2 ml of toluene-d_8. The NMR tube was sealed with a Precision Seal rubber septum cap and taken out of the glovebox and immersed in a cooling bath at −78°C. After equilibration at −78°C for 10 min, $^{[221]}$BTL (192 mg, 1.5 mmol, [$^{[221]}$BTL]/[IMes] = 100/1) in toluene-d_8 (0.3 ml) was added via a gas-tight syringe, and the NMR tube was brought into a 500-MHz NMR probe precooled to the desired polymerization temperature (20°, 10°, 0°, −10°, and −20°C, respectively). The conversion of the monomer was monitored by ^1H NMR at different time intervals until the conversion remained constant at each temperature. The equilibrium monomer concentration, $[\mathbf{M}]_{eq}$, was measured to be 2.55, 2.07, 1.65, 1.32, and 1.05 M for 20°, 10°, 0°, −10°, and −20°C, respectively (fig. S72). The van't Hoff plot of $\ln[\mathbf{M}]_{eq}$ versus $1/T$ gave a straight line with a slope of −1.69 and an intercept of 6.70 (fig. S73), from which thermodynamic parameters were calculated to be $\Delta H°_p = -14.1$ kJ mol^{-1} and $\Delta S°_p = -55.7$ J mol^{-1} K^{-1}, based on the equation $\ln[\mathbf{M}]_{eq} = \Delta H_p/RT - \Delta S°_p/R$. The T_c was calculated T_c = −20°, 30°, 60°, and 112°C at $[\mathbf{M}]_0$ = 1.0, 3.0, 5.0, and 10 M, respectively, on the basis of the equation $T_c = \Delta H°_p/(\Delta S°_p + R\ln[\mathbf{M}]_0)$.

Chemical recycling procedures

The chemical recycling experiment was performed in the presence of a catalyst, $La[N(SiMe_3)_2]_3$. In a glovebox under argon atmosphere, 1.0 g of pure cyclic PBTL (M_n ~ 100 kg/mol) was added to a sublimator, and $La[N(SiMe_3)_2]_3$ (1.0 mol %) in 0.5 ml of toluene was added. The sublimator was sealed, taken out of the glovebox, and immersed in the oil bath. The mixture was heated at 100°C for 24 hours, after which the reaction mixture was cooled to RT and colorless solid was obtained, which was confirmed to be the cleanly and quantitatively recycled monomer $^{[221]}$BTL by ^1H NMR analysis. Gram-scale depolymerization of PBTL was also performed at RT in the presence of an organic base catalyst (IMes). In a glovebox, 1.28 g of cyclic PBTL (M_n ~ 100 kg/mol) and 4.0 ml of toluene were added into a 20-ml vial, and IMes (1.0 mol%) in 1.0 ml of toluene was added. The PBTL was completely depolymerized into $^{[221]}$BTL in 10 min, monitored by ^1H NMR (fig. S75).

Thermal, mechanical, and rheological analysis

Melting transition temperature (T_m) and glass transition temperature (T_g) of purified and thoroughly dried polymer samples were measured by DSC on an Auto Q20, TA Instrument. All T_m and T_g values were obtained from a second scan (unless indicated otherwise) after the thermal history was removed from the first scan. The second heating rate was 10°C/min and cooling rate was 10°C/min. Decomposition temperatures ($T_{d,5\%}$) and maximum rate decomposition temperatures (T_{max}) of the polymers were measured by TGA on a Q50 TGA analyzer, TA Instrument. Polymer samples were heated from ambient temperatures to 700°C at a heating rate of 10°C/min. Values of T_{max} were obtained by the peak values from derivative (wt %/°C) versus temperature (°C) plots, while $T_{d,5\%}$ values were obtained by the temperatures at 5% weight loss from wt % versus temperature (°C) plots.

Film specimens suitable for DMA were prepared via solvent casting of concentrated polymer solutions in chloroform. Polymer solutions were solvent cast using a syringe into polytetrafluoroethylene (PTFE) molds and left to dry gradually at RT in open air for 24 to 48 hours and then moved to a 70°C oven for 48 hours, after which the films were extensively dried in a vacuum oven up to 100° or 140°C for 12 hours.

Storage modulus (E'), loss modulus (E''), and tan δ (E''/E') were measured by DMA on a Q800 DMA analyzer (TA Instruments) in a tension film mode at a maximum strain of 0.3 or 0.05% and a frequency of 1 Hz (complying with strain-sweep and frequency-sweep linearity analysis performed before sample testing). Specimens for analysis were generated via solvent casting of polymer materials in chloroform into PTFE molds (approximately 35 mm by 15 mm by 1.5 mm), dried, and cut down to a standard width (13 mm). Specimen length (5 to 10 mm) and thickness (0.40 to 0.60 mm) were measured for normalization of data by Q-series measurement software (TA Instruments). Test specimens were mounted to screw-tight grips (maximum 2 N). The samples were heated from −50° to 250°C at a heating rate of 3°C min^{-1}. The α-transition temperature was calculated as the peak maxima of the δ curve. Samples were tested

to the point of yield (amplitude of displacement, >20 mm) with measurements repeated for three specimens; the values reported are averaged from the measured data.

Tensile stress/strain testing was performed by an Instron 4442 universal testing system (50 N load cell) on dog bone–shaped test specimens (ASTM D638 standard; type V) prepared via slow-solvent evaporation. Concentrated polymer solutions in chloroform were solvent cast into PTFE molds (approximately 73 mm by 54 mm by 7 mm), thoroughly dried, and cut using an ASTM D638-5-IMP cutting die (Qualitest) to standard dimensions. Thickness (0.40 to 0.60 mm) and grip length (25 to 26 mm) were measured for normalization of data by the Bluehill measurement software (Instron). Test specimens were affixed into the pneumatic grip (maximum, 2 kN) frame at 0.208 MPa (N_2). Tensile stress and strain were measured to the point of material break at a grip extension speed of 5.0 mm/min at RT, with the measurements repeated more than three times, and the values reported are averaged from the measured data.

Computational details

All the DFT calculations were performed using the Gaussian 09 package (*43*). Geometry optimizations were performed using the BP86 GGA functional of Becke (*44*) and Perdew (*45*, *46*) with the standard split-valence basis set with a polarization function by Weigend and Ahlrichs (SVP keyword in Gaussian) (*47*) for the main atoms. Geometry optimizations were performed without symmetry constraints. Transition states were approached through a linear transit procedure using the forming bond as the reaction coordinate. All the geometries discussed in this work were confirmed as minima or transition states by frequency calculations. Moreover, intrinsic reaction coordinate calculations were performed to verify the connectivity of all transition states with their corresponding minima. Single-point energy calculations in solution were performed with the triple-ζ and one polarization function basis set proposed by the Ahlrichs (TZVP keyword in Gaussian) basis set. Solvent effects were included with the polarizable continuous solvation model using toluene and DMF as solvent (*48*, *49*). Reported energies are M06/TZVP//BP86/SVP electronic energies corrected with ZPEs, thermal energies, and entropy effects calculated at a temperature of 298 K and a pressure of 1354 atm, as suggested by Martin *et al.* (*50*). Cartesian coordinates were listed in table S3.

SUPPLEMENTARY MATERIALS

Supplementary material for this article is available at http://advances.sciencemag.org/cgi/content/full/6/34/eabc0495/DC1

REFERENCES AND NOTES

1. J. R. Jambeck, R. Geyer, C. Wilcox, T. R. Siegler, M. Perryman, A. Andrady, R. Narayan, K. L. Law, Plastic waste inputs from land into the ocean. *Science* **347**, 768–771 (2015).
2. World Economic Forum, Ellen MacArthur Foundation and McKinsey & Company, *The new plastics economy: Rethinking the future of plastics* (2016); www.ellenmacarthurfoundation.org/publications/the-new-plastics-economy-rethinking-the-future-of-plastics.
3. R. Geyer, J. R. Jambeck, K. L. Law, Production, use, and fate of all plastics ever made. *Sci. Adv.* **3**, e1700782 (2017).
4. M. Hong, E. Y.-X. Chen, Future directions for sustainable polymers. *Trends Chem.* **1**, 148–151 (2019).
5. X. Zhang, M. Fevre, G. O. Jones, R. M. Waymouth, Catalysis as an enabling science for sustainable polymers. *Chem. Rev.* **118**, 839–885 (2018).
6. D. K. Schneiderman, M. A. Hillmyer, 50th anniversary perspective: There is a great future in sustainable polymers. *Macromolecules* **50**, 3733–3749 (2017).
7. M. Hong, E. Y.-X. Chen, Chemically recyclable polymers: A circular economy approach to sustainability. *Green Chem.* **19**, 3692–3706 (2017).
8. G. W. Coates, Y. D. Y. L. Getzler, Chemical recycling to monomer for an ideal, circular polymer economy. *Nat. Rev. Mater.* **5**, 501–516 (2020).
9. H. Sardon, A. P. Dove, Plastics recycling with a difference. *Science* **360**, 380–381 (2018).
10. J.-B. Zhu, E. M. Watson, J. Tang, E. Y.-X. Chen, A synthetic polymer system with repeatable chemical recyclability. *Science* **360**, 398–403 (2018).
11. X. Tang, E. Y.-X. Chen, Toward infinitely recyclable plastics derived from renewable cyclic esters. *Chem* **5**, 284–312 (2019).
12. C. Jehanno, M. M. Pérez-Madrigal, J. Demarteau, H. Sardon, A. P. Dove, Organocatalysis for depolymerisation. *Polym. Chem.* **10**, 172–186 (2019).
13. X.-B. Lu, Y. Liu, H. Zhou, Learning nature: Recyclable monomers and polymers. *Chem. Eur. J.* **24**, 11255–11266 (2018).
14. J. M. Garcia, M. L. Robertson, The future of plastics recycling. *Science* **358**, 870–872 (2017).
15. Y. Zhu, C. Romain, C. K. Williams, Sustainable polymers from renewable resources. *Nature* **540**, 354–362 (2016).
16. A. Rahimi, J. M. García, Chemical recycling of waste plastics for new materials production. *Nat. Rev. Chem.* **1**, 0046 (2017).
17. M. Hong, E. Y.-X. Chen, Completely recyclable biopolymers with linear and cyclic topologies via ring-opening polymerization of γ-butyrolactone. *Nat. Chem.* **8**, 42–49 (2016).
18. M. Hong, E. Y.-X. Chen, Towards truly sustainable polymers: A metal-free recyclable polyester from biorenewable non-strained γ-butyrolactone. *Angew. Chem. Int. Ed.* **55**, 4188–4193 (2016).
19. J.-B. Zhu, E. Y.-X. Chen, Catalyst-sidearm-induced stereoselectivity switching in polymerization of a racemic lactone for stereocomplexed crystalline polymer with a circular life cycle. *Angew. Chem. Int. Ed.* **58**, 1178–1182 (2019).
20. A. Sangroniz, J.-B. Zhu, X. Tang, A. Etxeberria, E. Y.-X. Chen, H. Sardon, Packaging materials with desired mechanical and barrier properties and full chemical recyclability. *Nat. Commun.* **10**, 3559 (2019).
21. M. K. Kiesewetter, E. J. Shin, J. L. Hedrick, R. M. Waymouth, Organocatalysis: Opportunities and challenges for polymer synthesis. *Macromolecules* **43**, 2093–2107 (2010).
22. P. Olsén, K. Odelius, A.-C. Albertsson, Thermodynamic presynthetic considerations for ring-opening polymerization. *Biomacromolecules* **17**, 699–709 (2016).
23. J. Yuan, W. Xiong, X. Zhou, Y. Zhang, D. Shi, Z. Li, H. Lu, 4-Hydroxyproline-derived sustainable polythioesters: Controlled ring-opening polymerization, complete recyclability, and facile functionalization. *J. Am. Chem. Soc.* **141**, 4928–4935 (2019).
24. R. A. Smith, G. Fu, O. McAteer, M. Xu, W. R. Gutekunst, Radical approach to thioester-containing polymers. *J. Am. Chem. Soc.* **141**, 1446–1451 (2019).
25. M. Suzuki, K. Makimura, S.-i. Matsuoka, Thiol-mediated controlled ring-opening polymerization of cysteine-derived β-thiolactone and unique features of product polythioester. *Biomacromolecules* **17**, 1135–1141 (2016).
26. S. Mavila, B. T. Worrell, H. R. Culver, T. M. Goldman, C. Wang, C.-H. Lim, D. W. Domaille, S. Pattanayak, M. K. Mc Bride, C. B. Musgrave, C. N. Bowman, Dynamic and responsive DNA-like polymers. *J. Am. Chem. Soc.* **140**, 13594–13598 (2018).
27. T. J. Bannin, M. K. Kiesewetter, Poly(thioester) by organocatalytic ring-opening polymerization. *Macromolecules* **48**, 5481–5486 (2015).
28. C. G. Overberger, J. K. Weise, Anionic ring-opening polymerization of thiolactones. *J. Am. Chem. Soc.* **90**, 3533–3537 (1968).
29. X. Tang, A. H. Westlie, E. M. Watson, E. Y.-X. Chen, Stereosequenced crystalline polyhydroxyalkanoates from diastereomeric monomer mixtures. *Science* **366**, 754–758 (2019).
30. J. C. Worch, J. C. Worch, H. Prydderch, S. Jimaja, P. Bexis, M. L. Becker, A. P. Dove, Stereochemical enhancement of polymer properties. *Nat. Rev. Chem.* **3**, 514–535 (2019).
31. G. W. Coates, R. M. Waymouth, Oscillating stereocontrol: A strategy for the synthesis of thermoplastic elastomeric polypropylene. *Science* **267**, 217–219 (1995).
32. A. J. Teator, F. A. Leibfarth, Catalyst-controlled stereoselective cationic polymerization of vinyl ethers. *Science* **363**, 1439–1443 (2019).
33. H. Li, R. M. Shakaroun, S. M. Guillaume, J.-F. Carpentier, Recent advances in metal-mediated stereoselective ring-opening polymerization of functional cyclic esters towards well-defined poly(hydroxy acid)s: From stereoselectivity to sequence-control. *Chem. Eur. J.* **26**, 128–138 (2020).
34. E. Y.-X. Chen, Coordination polymerization of polar vinyl monomers by single-site metal catalysts. *Chem. Rev.* **109**, 5157–5214 (2009).
35. G. W. Coates, Precise control of polyolefin stereochemistry using single-site metal catalysts. *Chem. Rev.* **100**, 1223–1252 (2000).
36. H. H. Brintzinger, D. Fischer, R. Mülhaupt, B. Rieger, R. M. Waymouth, Stereospecific olefin polymerization with chiral metallocene catalysts. *Angew. Chem. Int. Ed.* **34**, 1143–1170 (1995).
37. L.-B. W. Lee, R. A. Register, Hydrogenated ring-opened polynorbornene: A highly crystalline atactic polymer. *Macromolecules* **38**, 1216–1222 (2005).
38. P. Corradini, F. Auriemma, C. De Rosa, Crystals and crystallinity in polymeric materials. *Acc. Chem. Res.* **39**, 314–323 (2006).

39. H. A. Brown, R. M. Waymouth, Zwitterionic ring-opening polymerization for the synthesis of high molecular weight cyclic polymers. *Acc. Chem. Res.* **46**, 2585–2596 (2013).
40. D. A. Culkin, W. Jeong, S. Csihony, E. D. Gomez, N. P. Balsara, J. L. Hedrick, R. M. Waymouth, Zwitterionic polymerization of lactide to cyclic poly(lactide) by using N-heterocyclic carbene organocatalysts. *Angew. Chem. Int. Ed.* **46**, 2627–2630 (2007).
41. G. O. Jones, Y. A. Chang, H. W. Horn, A. K. Acharya, J. E. Rice, J. L. Hedrick, R. M. Waymouth, N-heterocyclic carbene-catalyzed ring opening polymerization of ε-caprolactone with and without alcohol initiators: Insights from theory and experiment. *J. Phys. Chem. B* **119**, 5728–5737 (2015).
42. J. Roovers, Organic cyclic polymers, in *Cyclic Polymers*, J. A. Semlyen, Ed. (Kluwer Academic, ed. 2, 2000), pp. 347–384.
43. Gaussian 09, Revision D.01, M. J. Frisch, G. W. Trucks, H. B. Schlegel, G. E. Scuseria, M. A. Robb, J. R. Cheeseman, G. Scalmani, V. Barone, B. Mennucci, G. A. Petersson, H. Nakatsuji, M. Caricato, X. Li, H. P. Hratchian, A. F. Izmaylov, J. Bloino, G. Zheng, J. L. Sonnenberg, M. Hada, M. Ehara, K. Toyota, R. Fukuda, J. Hasegawa, M. Ishida, T. Nakajima, Y. Honda, O. Kitao, H. Nakai, T. Vreven, J. A. Montgomery Jr., J. E. Peralta, F. Ogliaro, M. Bearpark, J. J. Heyd, E. Brothers, K. N. Kudin, V. N. Staroverov, R. Kobayashi, J. Normand, K. Raghavachari, A. Rendell, J. C. Burant, S. S. Iyengar, J. Tomasi, M. Cossi, N. Rega, J. M. Millam, M. Klene, J. E. Knox, J. B. Cross, V. Bakken, C. Adamo, J. Jaramillo, R. Gomperts, R. E. Stratmann, O. Yazyev, A. J. Austin, R. Cammi, C. Pomelli, J. W. Ochterski, R. L. Martin, K. Morokuma, V. G. Zakrzewski, G. A. Voth, P. Salvador, J. J. Dannenberg, S. Dapprich, A. D. Daniels, Ö. Farkas, J. B. Foresman, J. V. Ortiz, J. Cioslowski, and D. J. Fox, Gaussian, Inc., Wallingford CT, 2009.
44. A. D. Becke, Density-functional exchange-energy approximation with correct asymptotic behavior. *Phys. Rev. A* **38**, 3098–3100 (1988).
45. J. P. Perdew, Density-functional approximation for the correlation energy of the inhomogeneous electron gas. *Phys. Rev. B* **33**, 8822–8824 (1986).
46. J. P. Perdew, Erratum: Density-functional approximation for the correlation energy of the inhomogeneous electron gas. *Phys. Rev. B* **34**, 7406–7406 (1986).
47. F. Weigend, R. Ahlrichs, Balanced basis sets of split valence, triple zeta valence and quadruple zeta valence quality for H to Rn: Design and assessment of accuracy. *Phys. Chem. Chem. Phys.* **7**, 3297–3305 (2005).
48. J. Tomasi, B. Mennucci, R. Cammi, Quantum mechanical continuum solvation models. *Chem. Rev.* **105**, 2999–3094 (2005).
49. V. Barone, M. Cossi, Quantum calculation of molecular energies and energy gradients in solution by a conductor solvent model. *J. Phys. Chem. A* **102**, 1995–2001 (1998).
50. R. L. Martin, P. J. Hay, L. R. Pratt, Hydrolysis of ferric ion in water and conformational equilibrium. *J. Phys. Chem. A* **102**, 3565–3573 (1998).

Acknowledgments: This work made use of the Central Instrument Facility of Colorado State University and polymer characterization instruments of E.Y.-X.C. and G. Miyake research groups. **Funding:** This work was supported, in part, by Colorado State University and by the U.S. Department of Energy, Office of Energy Efficiency and Renewable Energy, Advanced Manufacturing Office (AMO), and Bioenergy Technologies Office (BETO). This work was performed as part of the BOTTLE Consortium and funded under contract no. DE-AC36-08GO28308 with the National Renewable Energy Laboratory, operated by the Alliance for Sustainable Energy. The computational study used the resources of the King Abdullah University of Science and Technology Supercomputing Laboratory (KSL). **Author contributions:** C.S. and E.Y.-X.C. conceived the idea and designed the experiments. C.S. carried out the experiments, L.F. and L.C. performed and analyzed the DFT calculations, and M.L.M. contributed to elucidation of stereomicrostructures and stereocontrol mechanisms. C.S., M.L.M., L.F. and E.Y.-X.C. co-wrote the manuscript and participated in data analyses and discussions. All authors read and edited the manuscript. E.Y.-X.C. directed the project. **Competing interests:** E.Y.-X.C. and C.S. are inventors on a U.S. provisional application submitted by the Colorado State University Research Foundation, which covers the herein described polymers. M.L.M., L.C., L.F., and Z.-C.L. declare that they have no competing interests. **Data and materials availability:** All data needed to evaluate the conclusions in the paper are present in the paper and/or the Supplementary Materials. Additional data related to this paper may be requested from the authors.

Submitted 2 April 2020
Accepted 8 July 2020
Published 19 August 2020
10.1126/sciadv.abc0495

Citation: C. Shi, M. L. McGraw, Z.-C. Li, L. Cavallo, L. Falivene, E. Y.-X. Chen, High-performance pan-tactic polythioesters with intrinsic crystallinity and chemical recyclability. *Sci. Adv.* **6**, eabc0495 (2020).

ScienceAdvances

High-performance pan-tactic polythioesters with intrinsic crystallinity and chemical recyclability

Changxia Shi, Michael L. McGraw, Zi-Chen Li, Luigi Cavallo, Laura Falivene, and Eugene Y.-X. Chen

Sci. Adv. **6** (34), eabc0495. DOI: 10.1126/sciadv.abc0495

Science Advances (ISSN 2375-2548) is published by the American Association for the Advancement of Science. 1200 New York Avenue NW, Washington, DC 20005. The title *Science Advances* is a registered trademark of AAAS.